Model-based analysis and simulation of airflow control systems of ventilation units in building environments

Wu, Zhuang; Melnik, Roderick V.N.; Borup, Finn

Published in:
Building and Environment

Publication date:
2007

Document Version
Publisher's PDF, also known as Version of record

Available online at www.sciencedirect.com
ScienceDirect
Building and Environment 42 (2007) 203–217
BUILDING AND ENVIRONMENT
www.elsevier.com/locate/buildenv

Model-based analysis and simulation of airflow control systems of ventilation units in building environments

Zhuang Wu[a], Roderick V.N. Melnik[b,*], Finn Borup[c]

[a]Department of Control Engineering, Aalborg University, Fredrik Bajers Vej 7C, Aalborg, DK-9220, Denmark
[b]Mathematical Modelling and Computational Sciences, Wilfrid Laurier University, 75 University Avenue West, Waterloo, ON, Canada N2L 3C5
[c]OJ Electronics A/S, Stenager 13B, Sønderborg, DK6400, Denmark

Received 16 January 2004; received in revised form 25 May 2005; accepted 29 August 2005

Abstract

Model-based analysis and simulation of the airflow control system of ventilation units is of primary importance for the design and maintenance of the entire HVAC system in building environments. In this paper, we develop a mathematical model to simulate such airflow control systems. The model is implemented and a systematic analysis of the system is carried out, including its dynamic simulations in SIMULINK. The simulation results are compared with data obtained from analytical predictions as well as with experimental results available for a lab-scale ventilation unit. Finally, based on the combination of temperature and airflow regulations with conventional PI controllers, we provide the results of simulations of the entire ventilation unit control system for two different types of loading conditions.

Keywords: HVAC systems and building environments; Simulation; Ventilation unit; Air flow control

1. Introduction

Design, testing, operation, and management of heating, ventilation and air conditioning (HVAC) systems rely increasingly on simulation techniques. Such techniques together with model-based analysis of HVAC systems and validation methodologies provide an important tool helping the users to carry out thorough tests of the systems by emulating their performance on a computer.

HVAC systems are equipment usually implemented for maintaining satisfactory comfort conditions in buildings. The energy consumption as well as indoor comfort aspects of ventilated and air conditioned buildings are highly dependent on the design, performance and control of their HVAC systems and equipment [1]. A typical ventilation unit can be simulated by considering two major components: the thermal block and the airflow block. These components for controlling temperature and airflow are indispensable in the design of the entire control system. In our airflow model, we take into account all its major parts such as the AC motor, frequency converter, air fan, air filter, pressure sensor, and temperature sensor. Our goal is to develop a computational procedure based on the mathematical modeling of each such part and to couple them together in an efficient manner. Then, we will analyze/emulate the entire control system by adding a PI controller and validate the results with analytical predictions and experimental data.

We will also pay a special attention to different loading conditions which constitute different thermal comfort controlling objectives: the temperature of the air extracted from the room, and the temperature of the air exited of heat exchanger and supplied from the ductwork to room. These situations will require controlling the supply air temperature and the exhausted air temperature, respectively.

Note that HVAC systems are typically controlled by using a proportional plus integral (PI) control law. However, it is known from experiments for a lab-scale ventilation unit that the airflow control system exhibits

*Corresponding author. Tel.: +1 318 257 3198; fax: +1 318 257 3823.
E-mail address: rmelnik@wlu.ca (R.V.N. Melnik).

0360-1323/$ - see front matter © 2005 Elsevier Ltd. All rights reserved.
doi:10.1016/j.buildenv.2005.08.031

Nomenclature

D	diameter of duct, m	ΔP	pressure difference, Pa
L	length of duct, m	T	temperature, K
v	airflow velocity, m/s	V	volume of room, m^3
ρ	density, kg/m^3	A	area of the wall of room, m^2
		c_p	specific heat of air at constant pressure, J/kg K

non-linear operating characteristics which cause control performance to vary when operating conditions change. This explains why the control scheme applied to the airflow regulation is a PI controller which can ensure that the performance of the system is stable and accurate [2].

We organize this paper as follows. In Section 2 we provide a brief introduction to a typical ventilation unit that used in building environments, as well as to the controlling sequence and the concept of the entire regulation system. In Section 3 we develop mathematical models for each component of the airflow control system and present a computational procedure for dynamic simulations of the system. The experiment-based graphs are also presented in this section. In Section 4 we discuss the concept of airflow regulation systems based on the airflow model with conventional PI controller. The performance of the entire plant model is also illustrated here. In Section 5 we use our model to simulate several typical loading conditions important for the construction of the entire control loop. Conclusions are given in Section 6 of the paper.

2. The ventilation unit description and the concept of the entire control system

The ventilation unit is a one-piece unit manufactured for comfort ventilation. It consists of the direct driven supply air and exhaust air fans, air filters, the heat recovery section, AC motor, frequency converter and built-in control equipment controlled from a hand-held terminal with plain text display. Due to its microprocessor-based structure, the system can solve highly complicated tasks. When heating is required, the rotor speed will first increase in the heat recovery unit. This will allow heating the supply air even if the outdoor temperature is very low. The procedure takes place as a controlling sequence and the main parameters in this sequence are temperature and airflow. Therefore, a closed-loop control system controls (a) the outlet temperature from the Heat Recovery model and (b) the airflow of the supply and exhausted air from the Air Flow model. This system is applied with conventional PI controllers and is aimed at emulating the performance of the entire control system as shown in Fig. 1, which is inspired by [3]. The individual components within the ventilation unit for the airflow control system are specified in Table 1. For convenience, we also present them in a simplified diagrammatic way in Fig. 2.

3. Analysis and mathematical modeling

In Fig. 3 we illustrate the airflow model and its feedback loop designed for fulfilling the constant airflow control.

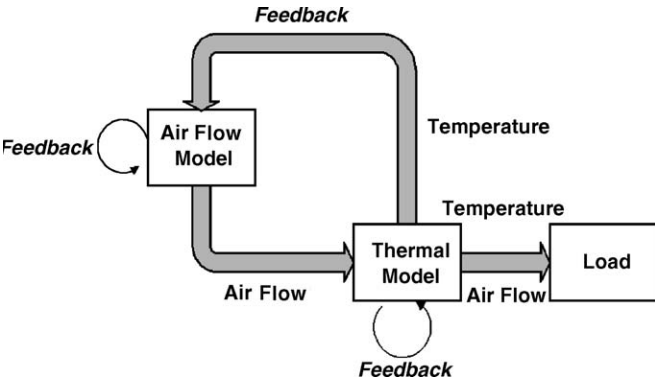

Fig. 1. Concept of the entire ventilation unit control system integrated with temperature control and airflow control.

Table 1
Components of ventilation unit

1		Outdoor air
3		Extract air
12		Exhaust air
14		Supply air
2, 13	PS-F	Pressure sensor for checking the filter status
4, 18	MP-AF	Airflow measurement probe (transmits input signals to the controller for controlling the speed of the fans to obtain the preset airflow rate)
5, 17	M	AC motor controlled in airflow control
6, 16	FC	Frequency converter for variable speed control of the fan motors
7, 19	Fan	Extracted and supply air axial fan
8	VSC	Variable speed-controlled rotary heat exchanger with purging operation (the speed of the rotor is supervised and controlled across temperature sensors in the outdoor air and exhaust air flows)
9	HT	Hand-held terminal for setting air flows, temperatures, control functions, hours in operation, etc. and alarms
10	TS-EA	Exhaust air temperature sensor
11, 23	Air Filter	Exhaust and supply air filter
15	TS-SA	In-duct supply air temperature sensor (located in the duct)
19	Fan	Supply air fan
20	RM-HE	Rotation monitor for checking the rotation of the heat exchanger
21	HEM	Heat exchanger drive motor
22	TS-OA	Outdoor air temperature sensor

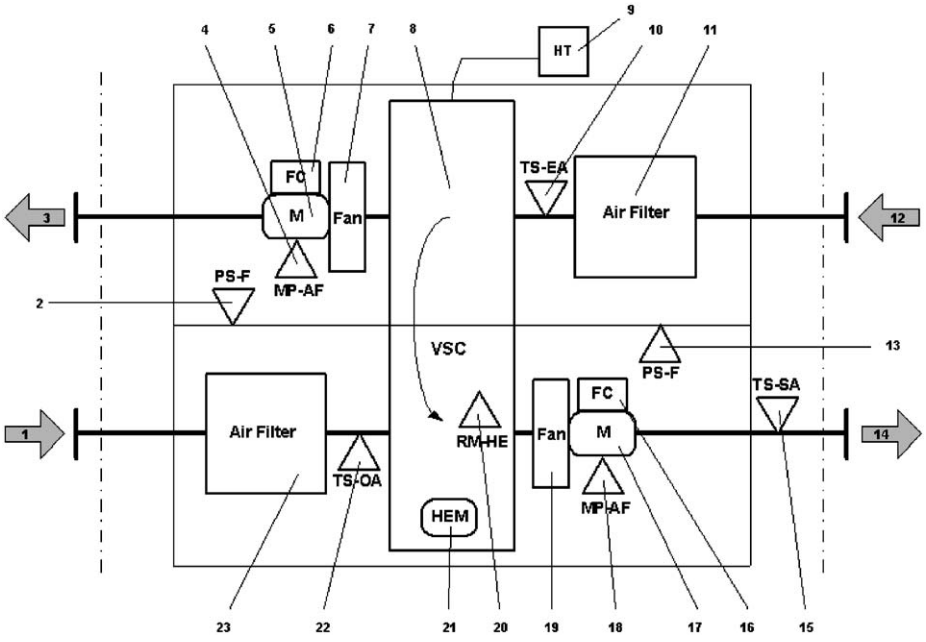

Fig. 2. Diagram of configuration and control system of ventilation unit.

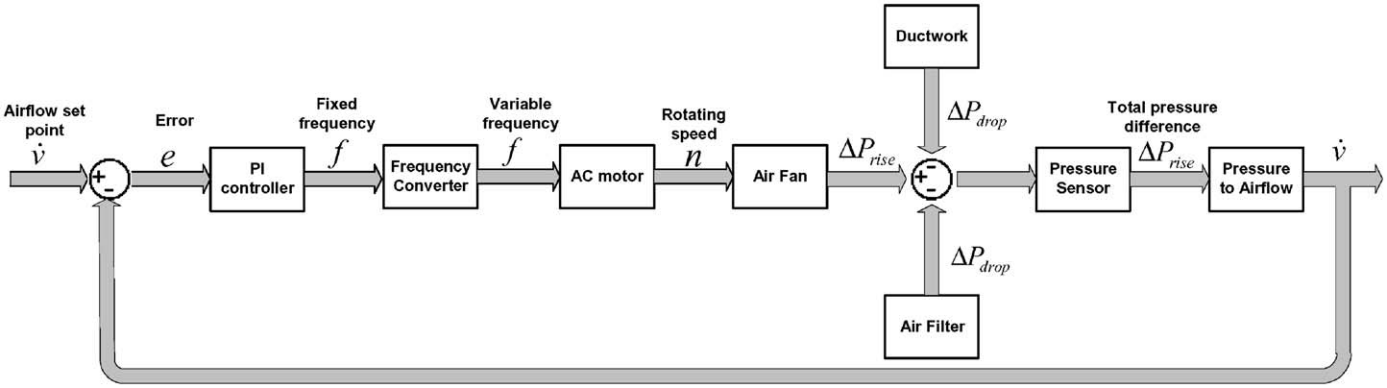

Fig. 3. The structure of building components within the airflow control system.

This control system contains a number of different models which are linked together to represent this complex system. The idea here is that individual models within a simulation may interact freely with other models. Alternatively, they may derive some of their inputs/outputs externally. Note that the required airflow is preset from a hand-held terminal display, and the air fan will rotate under the torque of shaft (provided by the AC motor driven by the frequency converter). Then, pressure drops over the filter and duct, rises from the fan, converted to the volumetric airflow and acts as a feedback to the controller. Now, our goal is to explain the essential physics and provide details on modeling and simulation for each component.

3.1. Frequency converter and AC motor

In the ventilation unit, the power for extracting and supplying air is provided by the AC motor. From [4], we know also that the speed of an asynchronous motor depends primarily on the pole number of the motor and the frequency of the voltage supplied. Furthermore, the amplitude of the voltage supplied and the load on the motor shaft also influence the motor speed. Therefore, a good methodology for asynchronous motor speed control would be just to change the frequency of the supply voltage. This is achieved by the frequency converter which allows us the conversion from the fixed voltage and frequency of the supply mains to a variable voltage/frequency. Given these facts, it is clear that the frequency converter and the AC motor play a critical role in the airflow control system.

Frequency converters allow us to use a ramp function when starting and stopping the motor. We will have the so-called soft start if we are able to avoid starting both fans at full speed with closed dampers. A side useful effect that is also well known is that in this way we reduce stresses on the fan transmission (belts) at the start [5]. Our simulation result for the frequency converter is presented in Fig. 5. It is

obtained from the function block given in Fig. 4 which is constructed for producing a ramp function.

In Fig. 5 we present the performance of the frequency converter with different required values. By analyzing the results, we conclude that irrespective to the input frequency, the model will produce a ramp function in which the saturation value equals to the input frequency. This result has been validated by experiments on the actual system.

The next step is to consider the motor. We limit our attention to squirrel-cage motors which are three-phase induction motors with a cage winding in the rotor. When AC voltage is applied to the stator, current flows through the windings. As a result, a rotating magnetic field will be developed in the space between stator and rotor and a relative speed will be produced between the rotating magnetic field and the rotor [6]. This motion generates an inductance current in the rotor windings resulting in a mechanical Lorentz force which in its turn is responsible for creating a torque.

Recall that the rotating synchronous speed of magnetic field of the motor can be determined as

$$n_S = 120\frac{f}{p}\ (r/\min), \tag{1}$$

where f (Hz) is the frequency from frequency converter and p is the number of the poles. The difference between the rotor speed n (rpm) and the synchronous speed n_S (rpm) of the rotating field is called slip s. It is dimensionless variable and we fixed this value at 3. Therefore, the rotor speed can

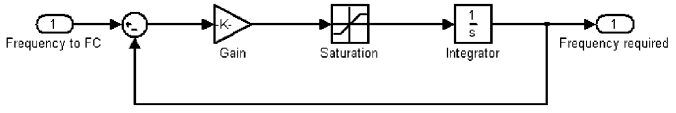

Fig. 4. Schematic block diagram of frequency converter model in SIMULINK.

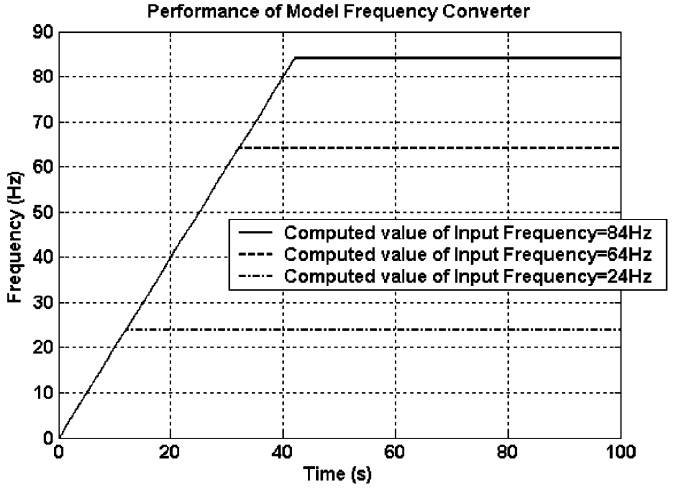

Fig. 5. Simulation of frequency converter model in SIMULINK for soft start by using a ramp function.

be defined as

$$n = 120\frac{f(1-s)}{p}\ (r/\min). \tag{2}$$

Based on the Eq. (2), the static relationship between the input and output of the motor can be established in terms of the functional block in SIMULINK. This block is given in Fig. 6.

As explained above, the rotational speed of the motor is computed statically in our procedure, but it varies with input conditions (e.g., the input frequency, slip, and pole).

3.2. Air axial fan

Axial flow coefficients ψ are derived from the static pressure rise across the fan measured on a flow stand [7]:

$$\psi = \frac{\Delta P_{\text{static}}}{\frac{1}{2}\rho v_{\text{tip}^2}}, \tag{3}$$

where ΔP_{static} (Pa) is the measurement of the difference in static pressures between the flow stand plenum and the downstream room where the fan flow is dumped. Finally, v_{tip} (m/s) is the fan tip velocity defined by Eq. (4):

$$v_{\text{tip}} = \pi d_{\text{tip}}\frac{N}{60}, \tag{4}$$

where d_{tip} (m) and N (r/m) are the fan diameter and fan speed, respectively.

In Fig. 7 a typical flow stand is given, where the plenum is located at position 1, the fan is installed between positions 2 and 3, and the downstream exit room is located at position 4. We follow the same idea as in [7] by first noting that ΔP_{static} from a fan test corresponds to $P_4 - P_1$. This value can be found in several steps. As pointed out in [7], as the flow accelerates from 1 to 2 in the plenum, the static pressure drops, and at the entrance to the fan at 2, the static pressure will drop by the amount equal to the dynamic pressure at that location (see the "static pressure profile" in Fig. 7).

The static pressure at 2 can be determined as

$$P_2 = P_1 - \tfrac{1}{2}\rho v_{\text{avg}^2}, \tag{5}$$

where ρ (kg/m^3) is the inlet density at the fan face on the streamline passing through the fan center, and v_{avg} (m/s) is the average air velocity into fan. Furthermore, the static

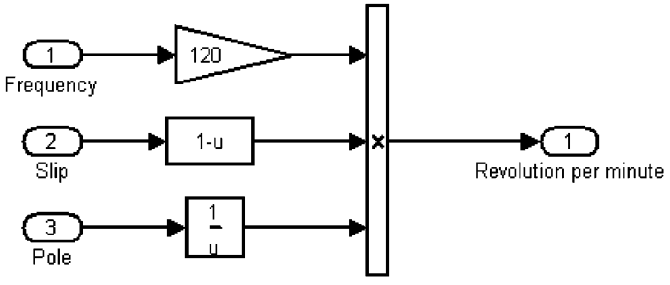

Fig. 6. Schematic block diagram of the AC motor model in SIMULINK.

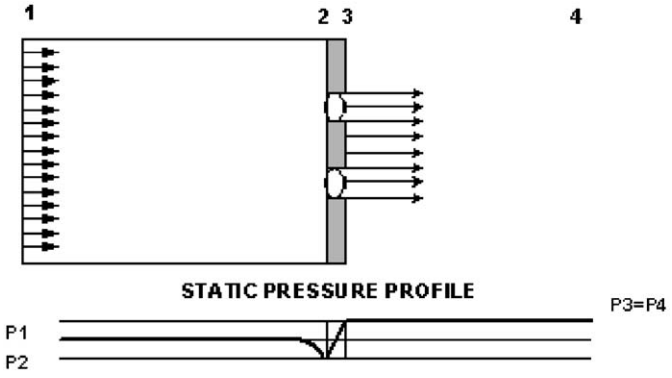

Fig. 7. Fan Test stand and static pressure profile [7].

pressure change across the fan can be determined as

$$\Delta P_{\text{fan,static}} = P_3 - P_2. \tag{6}$$

At the fan exit of 3, the static pressure P_3 is equal to the static pressure in the exit room P_4, giving that $P_3 = P_4$. Similar to [7] we combine Eqs. (5) and (6) to get, the static pressure rise across the fan:

$$\begin{aligned}\Delta P_{\text{fan,rise}} &= P_4 - P_2 = P_4 - P_1 + \tfrac{1}{2}\rho v_{2^2} \\ &= \Delta P_{\text{static}} + \tfrac{1}{2}\rho v_{2^2}.\end{aligned} \tag{7}$$

Finally,

$$\begin{aligned}P_{\text{total}} = \Delta P_{\text{fan,rise}} &= \frac{1}{2}\rho v_{\text{tip}^2}\psi + \frac{1}{2}\rho v_{\text{avg}^2} \\ &= \frac{1}{2}\rho\left[\pi d_{\text{tip}}\frac{N}{60}\right]^2\psi + \frac{1}{2}\rho\left[\frac{\dot{v}}{A_{\text{fan}}}\right]^2,\end{aligned} \tag{8}$$

where P_{total} is the total pressure difference between input and output, A_{fan} (m^2) is the annular swept area of the fan (in which the fan hub should be excluded).

From a practical point of view, the axial flow coefficients ψ can be determined through experiments based on a lab-scale ventilation unit (e.g., by using pressure sensors located at front and rear side of fan). In what follows, we assume that ψ is a constant independent of time and temperature. By combining (3) and (4), we evaluate ψ as follows:

$$\psi = \frac{\Delta P_{\text{static}}}{\frac{1}{2}\rho(\pi d_{\text{tip}})^2[2f(1-s)/p]^2}. \tag{9}$$

In Fig. 8 we compare the results obtained according to the procedure described above with average value of ψ and the data obtained from experiments. This concludes the definition of all the parameters that we need for the description the physical phenomena related to pressure rise across the air axial fan. The functional block for the fan is constructed on the basis of Eq. (8) and one can emulate the performance of the fan with the developed model. Fig. 9 illustrates the static relationship between the output and the input airflow, the density of the air, and the properties of the fan (such as diameter, pressure coefficient, etc.).

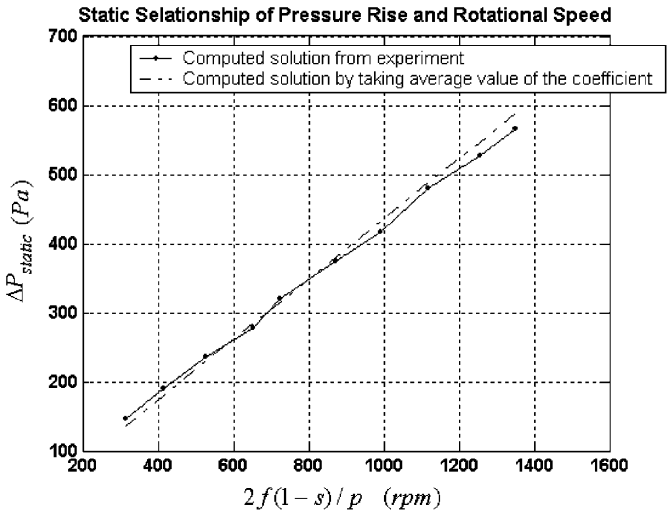

Fig. 8. Comparison of the pressure rise obtained from experiments and the data computed from the equation with average value coefficient.

3.3. Duct

The analysis of the duct in the ventilation unit is reduced to the thermodynamic analysis of incompressible gas flow in a duct [5]. For convenience, it is customary to denote the point at the beginning and the end of the duct by 1 and 2, respectively. Since there is no mechanical power, we follow a standard procedure writing the energy balance equation for steady-state flow as follows:

$$h_1 + \tfrac{1}{2}v_{1^2} + gz_1 = h_2 + \tfrac{1}{2}v_{2^2} + gz_2, \tag{10}$$

$$h_2 - h_1 = \int_1^2 T\,\mathrm{d}s + \frac{1}{\rho}(p_2 - p_1). \tag{11}$$

We denote by $\Delta p = \rho\int_1^2 T\,\mathrm{d}s$ the entropy generation given as pressure loss. As a result, our model can be rewritten in the following customary form:

$$p_1 + \tfrac{1}{2}\rho v_{1^2} + \rho g z_1 = p_2 + \tfrac{1}{2}\rho v_{2^2} + \rho g z_2 + \Delta p. \tag{12}$$

We limit ourselves to a straight duct where $z_1 = z_2$ and to the uniform cross-sectional area is uniform (that is where $v_1 = v_2$). This gives that $\Delta p = p_1 - p_2 > 0$. Furthermore, Δp is the duct pressure loss resulted from the entropy generation. Hence, given the above simplifications we determine the pressure loss as follows:

$$\Delta P_{\text{loss,duct}} = \lambda\frac{L}{D}\frac{\rho v^2}{2}, \tag{13}$$

where λ is the friction factor which can be determined as highlighted below, v is the average air velocity flow through the duct (m/s), ρ is the density of air inside duct (kg/m^3), other parameters are specified in Nomenclature [8].

For a *laminar* flow ($Re \leqslant 2300$), the friction factor λ is

$$\lambda = 64/Re, \tag{14}$$

where $Re = \rho v D/\mu$, μ is absolute viscosity coefficient which is defined in Table 2.

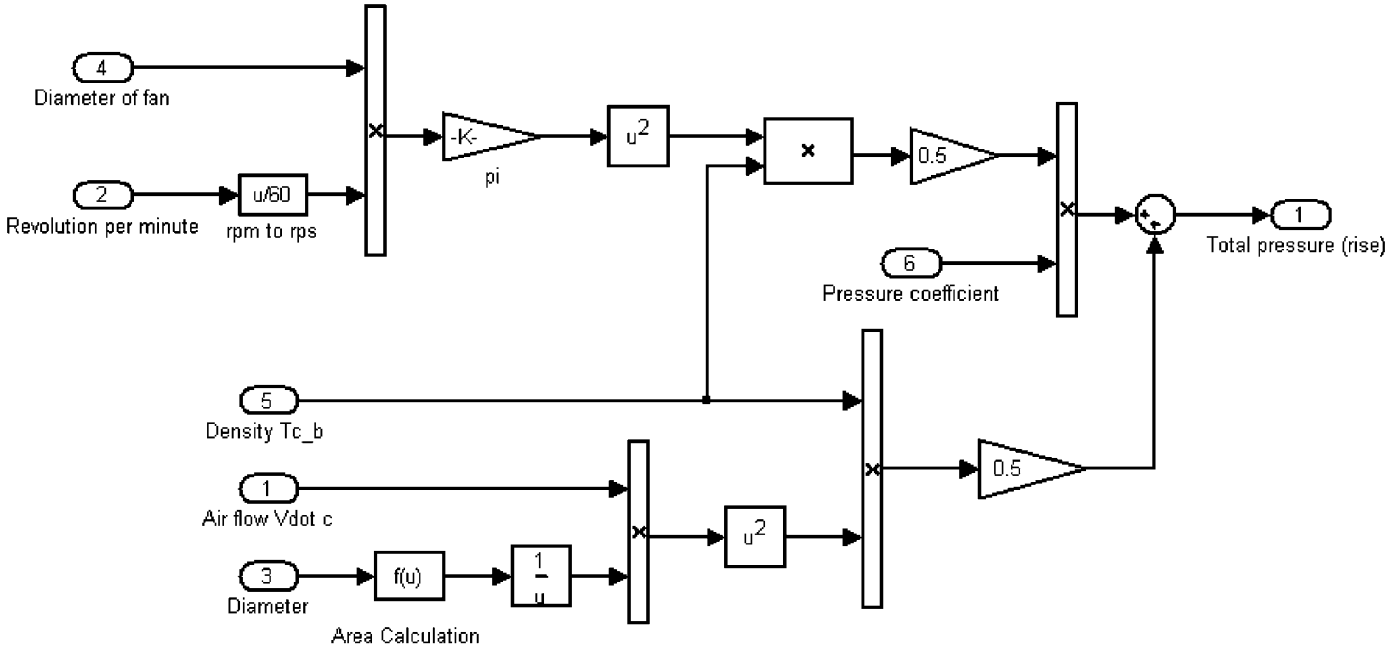

Fig. 9. Schematic block diagram of axial fan model in SIMULINK.

Table 2
Properties of air at atmospheric pressure [8]

T K	ρ kg/m	c_p kJ/kg °C	$\mu \times 10^5$ kg/m s	$v \times 10^6$ m^2/s	k W/m °C	$\alpha \times 10^4$ m^2/s	Pr Dimensionless
250	1.4128	1.0053	1.5990	11.31	0.02227	0.15675	0.722
300	1.1774	1.0057	1.8462	15.69	0.02624	0.22160	0.708

For a *turbulent* flow ($Re > 3500$), the friction factor λ is

$$\frac{1}{\sqrt{\lambda}} = -2\log\left[\frac{e}{3.72D} + \frac{2.54}{Re^{0.901}}\right]. \quad (15)$$

As follows from (15), the friction factor depends not only on the Reynolds number, but also on the duct wall relative roughness e/D, (e is the average height of the roughness in the duct wall). The value of e is given in Table 3.

In the transient regime where $2300 < Re < 3500$, the flow may be laminar or turbulent, and we use the following formula for the evaluation of λ:

$$\lambda = \frac{\lambda_{2300}(3500 - Re) + \lambda_{3500}(Re - 2300)}{3500 - 2300}, \quad (16)$$

where λ_{2300} and λ_{3500} are the calculated λ values at $Re = 2300$ and $Re = 3500$, respectively.

Pressure drop due to the local resistance is determined as

$$Z = \zeta \frac{v^2}{2}\rho, \quad (17)$$

where ζ is the local hydraulic coefficient (sometimes referred to as the local friction resistance factor). This coefficient depends on the geometrical shape of the ductwork and flow path through the various fittings used in duct systems [5].

Table 3
The surface roughness factor e [5]

Duct type	Material	e (10^{-3} m)
Seamless ducts	Steel	0.045
Seamless ducts	Aluminum	0.045
Seamless ducts	Plastics	0.01

Hence, the pressure loss and the corresponding resistance height are the sum of the friction losses and individual resistances:

$$\Delta P_{\text{duct,loss}} = \left(\lambda\frac{L}{D} + \sum\zeta\right)\frac{\rho v^2}{2} = \left(\lambda\frac{L}{D} + \sum\zeta\right)\frac{\rho}{2}\left(\frac{\dot{v}}{A}\right)^2. \quad (18)$$

The duct model is implemented through the function block construction in SIMULINK as shown in Fig. 10 based on (18). It can be seen on this block diagram that the output of pressure drop is determined by the geometrical size of duct,

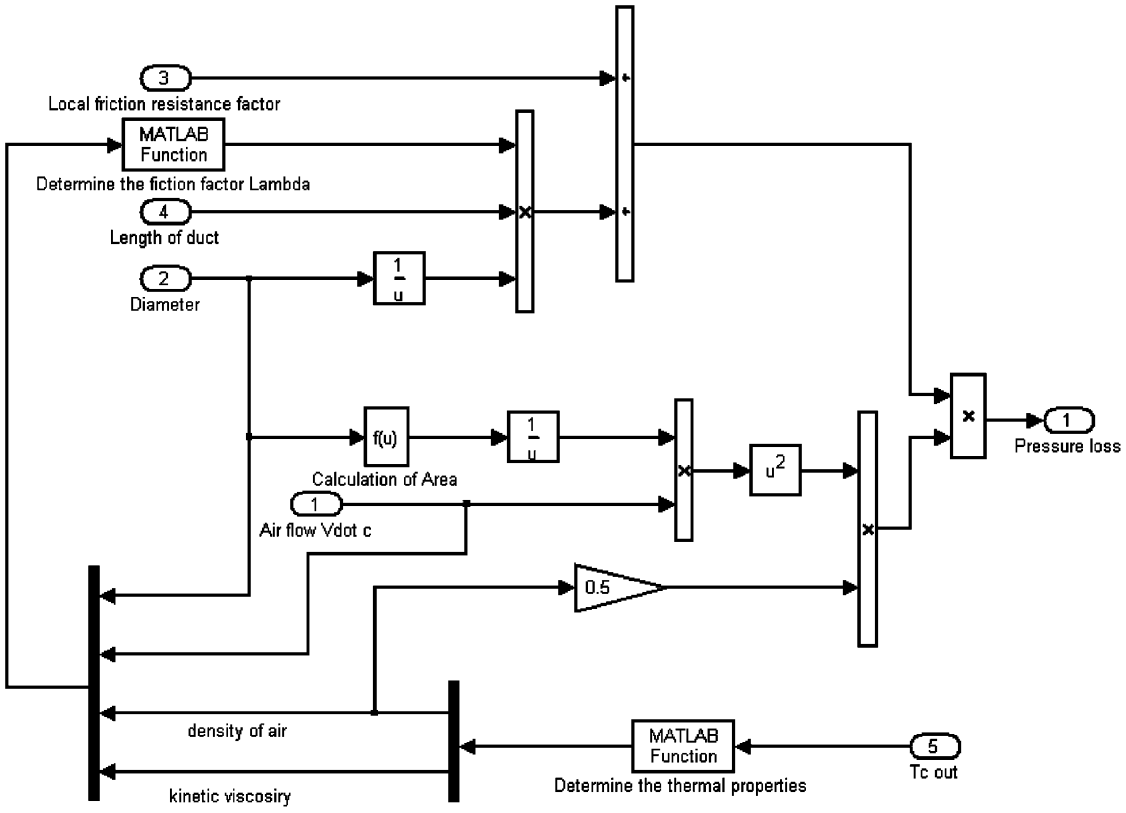

Fig. 10. Schematic block diagram of duct model in SIMULINK.

friction resistance factor, airflow, temperature, and thermal properties of the air inside duct.

3.4. Air filter

A pressure drop, induced by the airflow through the filter, varies with the temperature of flowing air. The faster the velocity of the airflow is, the bigger the pressure difference over the filter will be. The pressure drop can be calculated as follows:

$$\Delta P_{\text{pressure,drop}} = C_{\text{f}} \frac{1}{2} \rho_{\text{f}} v^2 = C_{\text{f}} \rho_{\text{f}} \frac{1}{2} \left[\frac{\dot{v}}{A_{\text{duct}}} \right]^2, \tag{19}$$

where $\Delta P_{\text{pressure,drop}}$ is the pressure drop over the filter (Pa), C_{f} is the pressure loss coefficient of filter (a filter material characteristic), v is the average velocity of air cross the filter (m/s), ρ_{f} is the density of filter material (kg/m^3). The coefficients C_{f} and ρ can be determined experimentally. In Fig. 11 we show comparison results between the data from experiments and the data obtained from theoretical predictions by taking the average value. The two curves coincide with each other quite well. Observed differences at some points may be attributed to inaccuracy of experimental equipment.

In Fig. 12 we present a SIMULINK implementation of this model. The function block is the block for the computation of the pressure drop over the filter. As

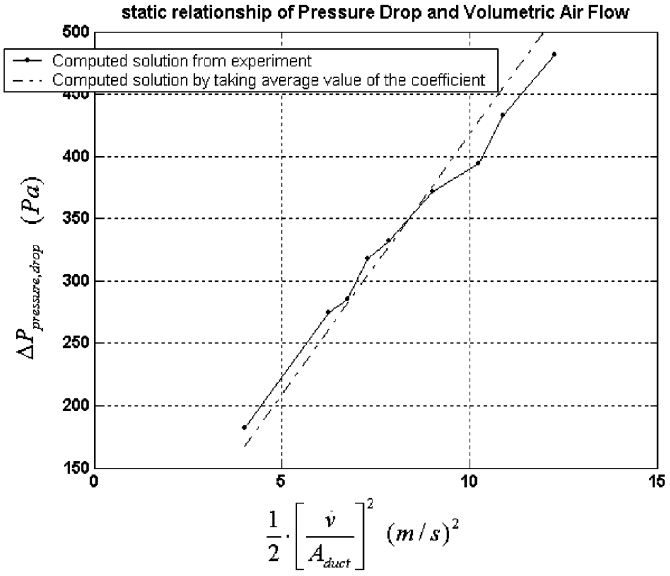

Fig. 11. Comparison of pressure drop obtained from experiments and computed from the equation with average value of coefficient.

expected, the input airflow and physical properties of the filter play an important role in the simulated output.

3.5. Pressure sensor

The final component is the pressure sensor which is an indispensable element in the design. The decision making in

the system is based on the controller revaluation of the difference between the required airflow and feedback airflow. The main purpose of the pressure sensor is to sense the output pressure which will be converted to airflow (we will focus on this issue in some further details in the next section).

The dynamic model for the pressure sensor can be given as follows:

$$\Delta P_{\text{out}} = \frac{1}{\tau}\int (\Delta P_{\text{in}} - \Delta P_{\text{out}})\,\mathrm{d}t. \tag{20}$$

The time constant τ in (20) represents the reacting effectiveness of the pressure sensor. In most realistic applications, the sensor has very short time delay and as a rule it responds very quickly. In order to decrease the computational cost in emulating the entire system the time constant of the pressure sensor can be neglected.

4. Control system construction and simulation results

When the ventilation unit is installed in building environments, the volumetric airflow is usually set directly from a hand-held terminal display. If we link all models that we have described in the previous section, we can find the output of the plant system in terms of the pressure difference, and our next step will be to establish a relationship between the pressure difference and the volumetric airflow. The equation connecting these two quantities can be written as follows:

$$\dot{v} = \sqrt{\frac{\Delta P_{\text{total}}}{c_1} + c_2} - \sqrt{c_2}, \tag{21}$$

where c_1, c_2 are constants taken as $c_1 = 3003$ and $c_2 = 0.000782$ emperically, ΔP_{total} (Pa) is the total air pressure (sum of the dynamic pressure and static pressure, the difference between the total pressure of the airflow out of the ventilator, and the total pressure of the air flow that enters the ventilator).

In Fig. 13 we present the function block developed on the basis of (21). This block acts as a feedback conversion component within the entire control system.

In the situation we consider here the PI control should be adequate, in particular when the process dynamics is essentially first order. A proportional controller will help to reduce the rise time and also will reduce the steady-state error. We can use the proportional gain parameter for proportional adjustments. The integral feedback loop will provide a corrective force that can eliminate tracking error. Since the integral force is proportional to the tracking error and increases linearly with time, the integral adjustments can be made with integral gain constant. A certain amount of trial and error is required for adjusting proportional and integral gain values, with an interactive computer simulation before a satisfactory design is obtained. In our particular example, of the airflow control system, the proportional gain was set at 0.003, while the integral gain was set at 20 (see Fig. 14).

The final ventilation control system is a multi-input-multi-output (MIMO) system, and the control scheme for this system can be evaluated by using a simulation which comprises of several subsystems and control loops interconnected with each other within the MATLAB environment. Those feedback control loops can then be applied in the final product as we run software in a real-time embedded processor due to robustness of the controller and simplicity of tuning the parameters. Fig. 15 shows the

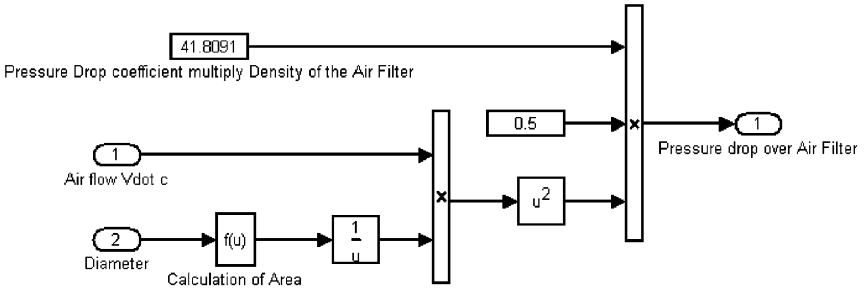

Fig. 12. Schematic block diagram of air filter model in SIMULINK.

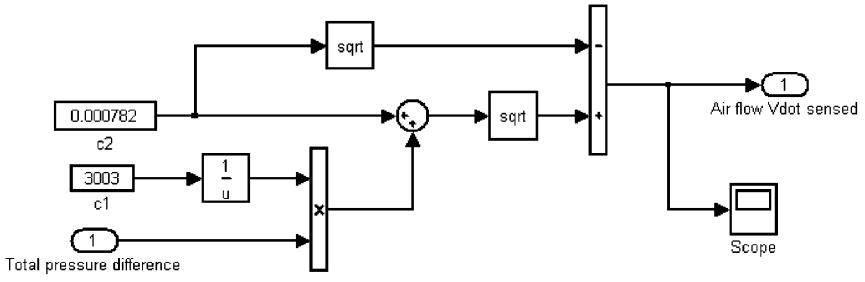

Fig. 13. Schematic block diagram for conversion from pressure to airflow (feedback gain) in SIMULINK.

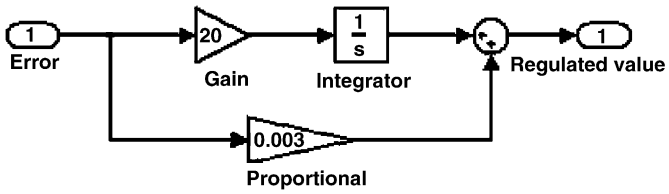

Fig. 14. Schematic block diagram of PI controller for airflow control system.

concept and overview of constant airflow control system, whose idea is inspired by [3].

In Fig. 16 we present the function block for the airflow plant model by adding a PI controller in SIMULINK.

Now, we are in a position to present our simulation results Fig. 17 for each function block model within the system which is implemented based on the structure of Figs. 3 and 15 when subjected to the test data listed in Table 4. In this context, 1. is the set-point, 2. is the output temperature from the heat exchanger, 3. is the density of air with bulk temperature, 4. is the diameter of the duct, 5. is the number of poles of the AC Motor, 6. is the slip of the AC Motor, 7. is the diameter of the air fan, 8. is the friction resistance factor inside duct, 9. is the length of the duct, 10. is the pressure coefficient of the air fan. The test data contains real measurements, estimations and computations. We note here that the thermal properties of air such as viscosity, thermal conductivity, and density vary considerably with temperature. Such property-variation effects at a particular flow cross section can be compensated for by evaluating some (or all, if necessary) properties at specified reference temperature with respect to the bulk temperature.

The analysis shows that the reacting effectiveness of the simulation result is around 40 s, but the saturation value is decided by the corresponding setpoint precisely. The process of reaching the steady state from initial conditions will proceed through a peak that will not be beyond the maximum airflow value. Comparisons with the experimental results for the ventilation unit show that the model can predict main features of the system dynamics. When the user sets the required value, the program embedded inside the mastercontroller will control the input frequency to the frequency converter. In this way, the rotating speed of the fan to produce the airflow can be controlled, and during this process the airflow will reach a value that is higher than the setpoint, after which it will go gradually to the steady state.

We have varied the set-point airflow rate in sequence of 0.25, 0.30, 0.35 m^3/s within the limit of the maximum airflow of system, in order to provide excitations similar to the actual airflow control and to facilitate a rigorous assessment of the controller. Fig. 18 shows the variation in the steady state airflow and the reacting time constant during the test data. The results are given to compare the performance for the three different conditions. These results were validated by comparing the behavior of the

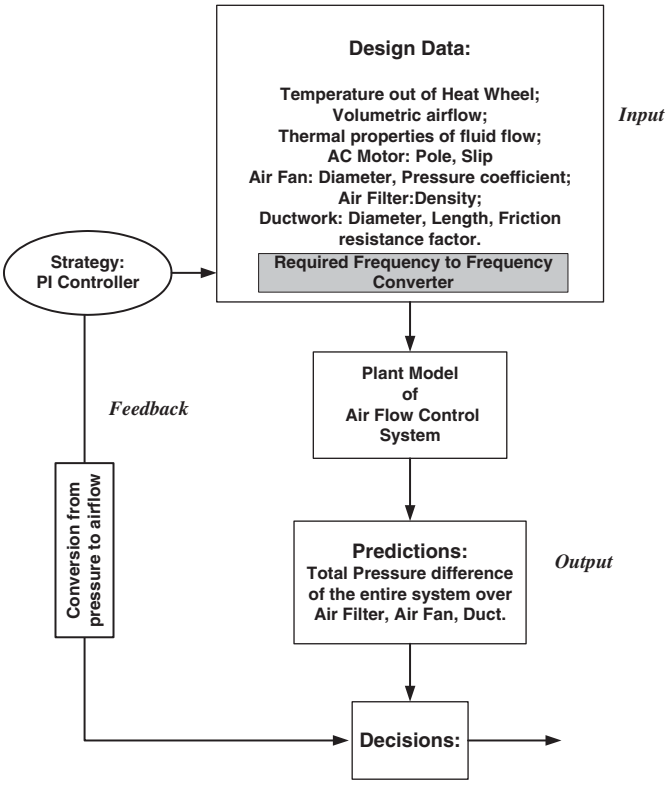

Fig. 15. Concept and overview of the constant air flow control system.

model with the measurements and observed behavior of a real system. Note that if the set-point is beyond the maximum airflow, the output will not reach that value and stay at the maximum level to protect the system.

5. Modeling and simulation of loading conditions

The ventilation unit is installed in the building environments via a ductwork. Therefore, in order to fulfill the controlling strategy for temperature control and airflow control, the issue related to the ventilating air itself needs to be investigated. There are two kinds of loading conditions to the plant model of ventilator. Firstly, the air inside the room can serve as a load at the entrance of the extracted air duct for ventilation (in order to implement the exhausted air temperature control). Secondly, the air inside the duct can serve as a load at the exit of the heat exchanger for ventilation (in order to implement the supply air temperature control). The mathematical model for the heat exchanger has been discussed elsewhere [9] and we do not touch upon this issue here.

For a constant exhaust air temperature control system, the unit should keep the exhaust air temperature constant, let us say, for example, that the exhausted air temperature should be controlled at 21 °C (see Fig. 19). Therefore, we need to analyze how the room air reacts with the ventilator. It is easy in this case to develop a mathematical model to simulate the system performance. The air temperature of a room at any given time can be given by a heat-balance

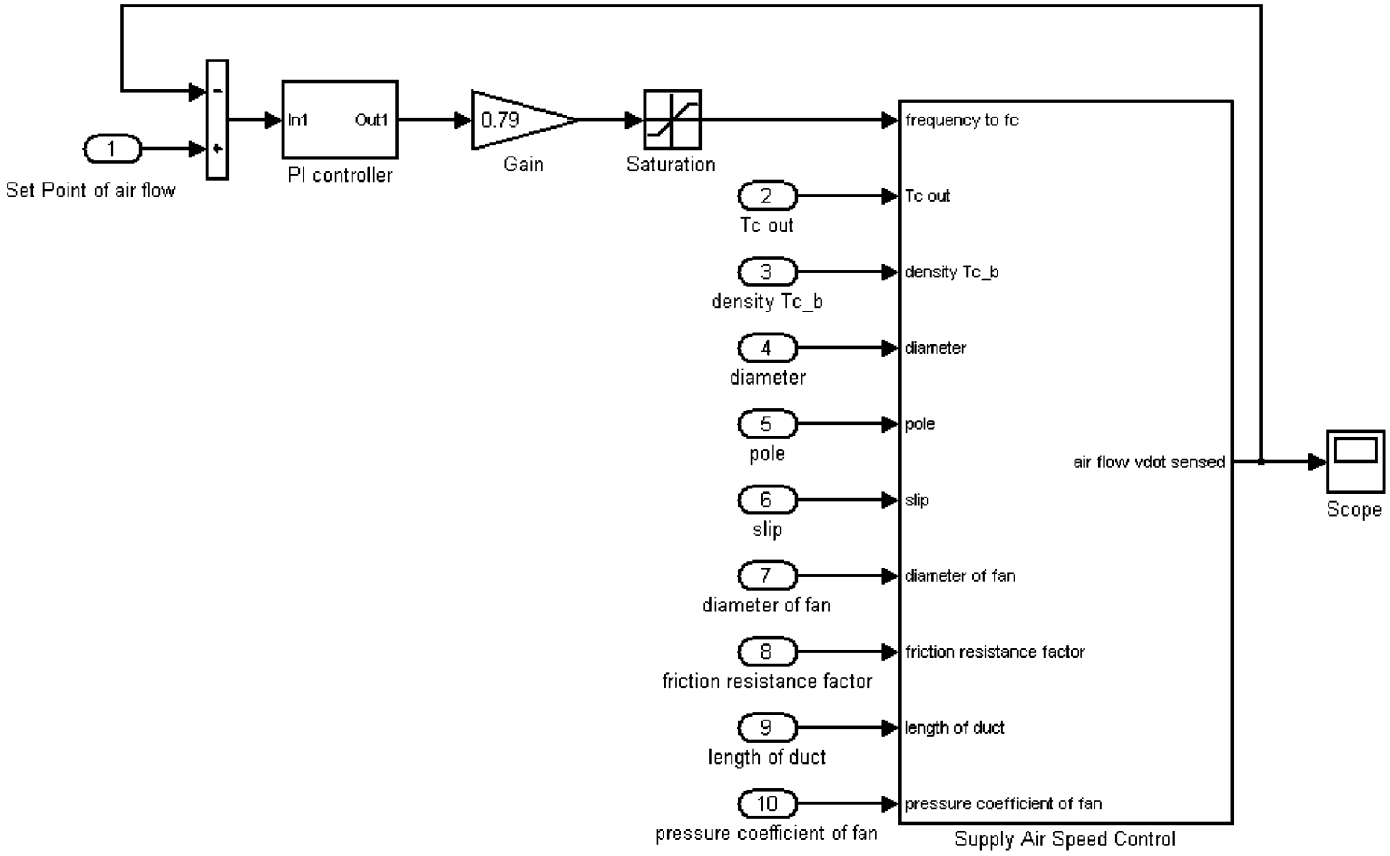

Fig. 16. Diagram of block surface for constant airflow control system in SIMULINK.

equation [5]:

$$\sum_{j=1}^{N}(A_j q_{c,j}) + \Phi_v + \Phi_{ic} + \Phi_{hc} + \Phi_{heater} = c_{p,indoor} M_R \frac{\partial T_{indoor}}{\partial t}, \quad (22)$$

where the heat flux exchanged by convection at each wall element is $(A_j q_{c,j})$, A_j is the area of wall element, $q_{c,j}$ is the convective heat flux, Φ_v is the heat flow exchanged by ventilation, Φ_{ic} denotes the convective part of heat flow due to internal heat gains from people, lights, appliances, infiltration, etc., Φ_{hc} is the convective part of heat flow due to the HVAC system, Φ_{heater} is the heat flow from the heater, and the variation of energy in the room air is $c_{p,indoor} M_R \frac{\partial T_{indoor}}{\partial t}$. Here, T_{indoor} is the temperature of the indoor air (K), M_R is the mass of air and $c_{p,indoor}$ is specific heat of indoor air, while Φ_{ic} and Φ_{hc} can be neglected in practice.

Therefore, the dynamic model for the room temperature can be written as follows:

$$c_p V_R \rho \frac{\partial T_{indoor}}{\partial t} = \lambda_{wall} \cdot A(T_{outdoor} - T_{indoor}) + \dot{v}_c \rho_c c_{p,c}(T_{h,in} - T_{c,out}) + \Phi_{heater}, \quad (23)$$

where $T_{outdoor}$ is the temperature of outside door air (K), $T_{c,out}$ is the temperature of supply air from the heat recovery section (K), $T_{h,in}$ is the temperature of exhausted air (K), V_R is the volume of the room (m^3), ρ_R is the density of the air in the room (kg/m^3), λ_{wall} is the heat conduction coefficient of the wall (W/m K), $\dot{v}_c$ is the volumetric airflow of cold air (m^3/s), ρ_c is the density of cold air from the heat recovery section (kg/m^3), $c_{p,c}$ is the specific heat of cold air from the heat recovery section (J/kg K), while other parameters are specified in Nomenclature. In Fig. 20 we present the simulation function block for the room air model constructed in SIMULINK.

For the room air model, the main affecting factors are airflow, the heat conduction coefficient of the wall, the volume of the room and whether the heater is on or off. The comparison of the performance of the model of room air under different conditions are schematically illustrated in Fig. 21. The results were obtained by varying the above dominant factors.

More specifically, there are three detection cases of operating conditions to compare the simulation performance with variable inputs. The initial condition of the room temperature was set at 288 K.

Case No. 1: The heater is off, while the heat conduction coefficient is very small 0.001, similar to that of an insulated occupant.

Case No. 2: The heater is on, while the energy is 100 J, but the heat conduction coefficient is big 2.000 (in which case it is easy to transfer energy).

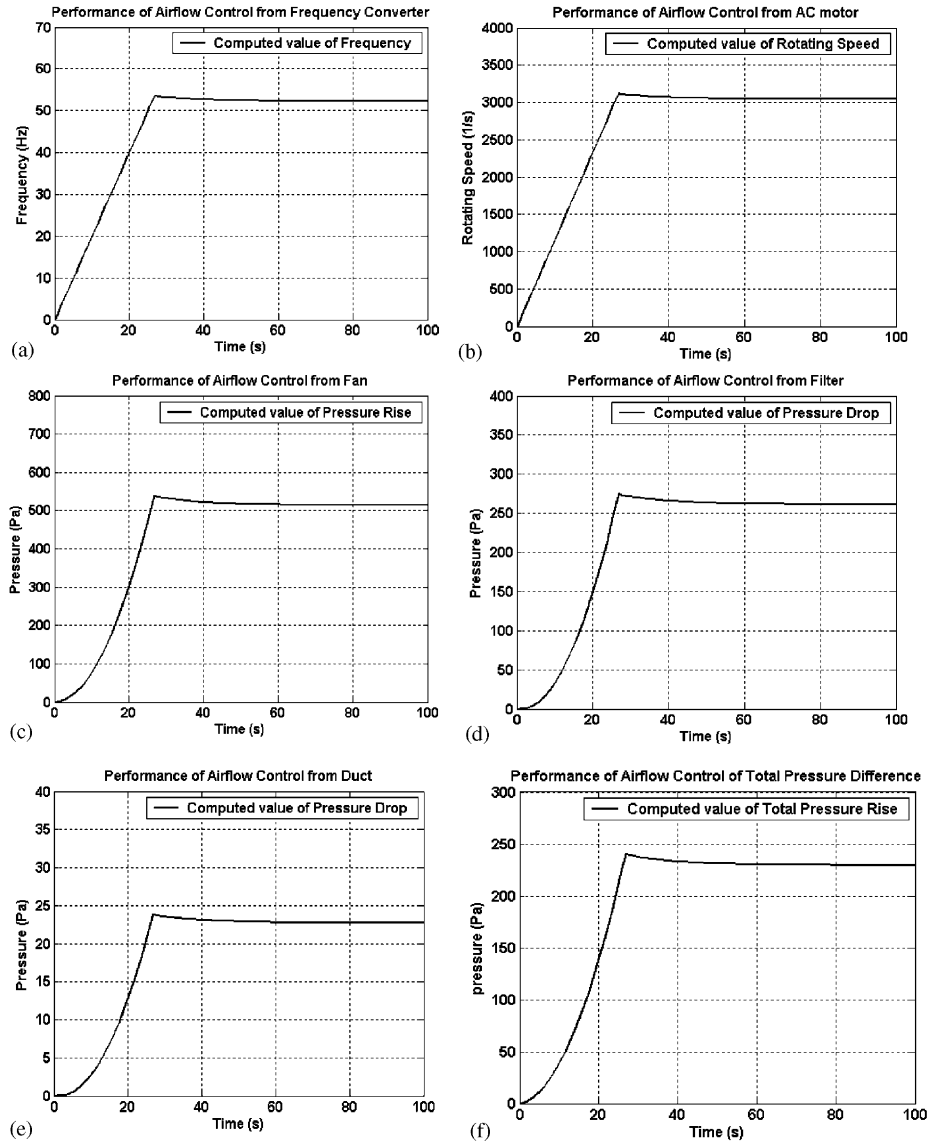

Fig. 17. Response of (a) Frequency converter, (b) AC motor, (c) air fan, (d) air filter, (e) duct, (f) computation of total pressure in SIMULINK within airflow control system.

Table 4
Parameters specifications for constant air flow control system at a specific condition

1	0.35	m^3/s
2	20	°C
3	1.2542	kg/m^3
4	0.3	m
5	2	Dimensionless
6	0.03	Dimensionless
7	0.27	m
8	0	Dimensionless
9	1	m
10	0.4362	Dimensionless

Case No. 3: The heater is off in the insulated occupant situation, while the airflow from the ventilator increases from 0.25 to 0.35.

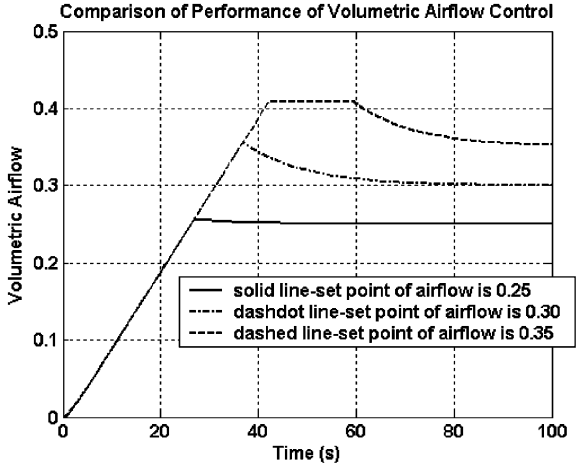

Fig. 18. Control system detection under three kinds of conditions.

From analysis of these three cases, the following conclusions can be reached. Within the same period of time, temperature will reach the highest level when the heater is on, even though the heat conduction coefficient is big. Temperature response effectiveness increases when airflow increases with specified heat conduction coefficient.

Let us consider now a different situation. As we know, the temperature required in the supply air ducting is displayed while the controller is keeping the supply air temperature constant (again, it is assumed that a heater will be required). Let us say, in this case, the supply air temperature should be controlled at 19 °C (see Fig. 22).

For the constant supply air temperature regulation system, we need to analyze how the duct air reacts with the ventilator. Again, this can be done easily by developing a mathematical model to simulate the system performance. The air temperature inside the duct at any given time can be given by the following heat-balance equation:

$$\dot{Q}_{\mathrm{hr}} + \dot{Q}_{\mathrm{heater}} = c_{\mathrm{p,s}} V_{\mathrm{induct}} \frac{\mathrm{d}T_{\mathrm{s}}}{\mathrm{d}t}, \tag{24}$$

where $\dot{Q}_{\mathrm{hr}}$ is the convective part of the heat flux due to the heat recovery wheel (W), $\dot{Q}_{\mathrm{heater}}$ is the heat flow from the heater equipped inside duct (W), $c_{\mathrm{p,s}}$ is the specific heat of

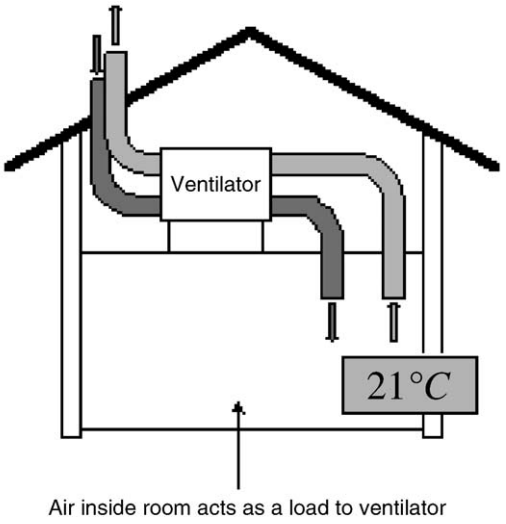

Fig. 19. Air inside room being a load to ventilation unit for exhausted air temperature regulation.

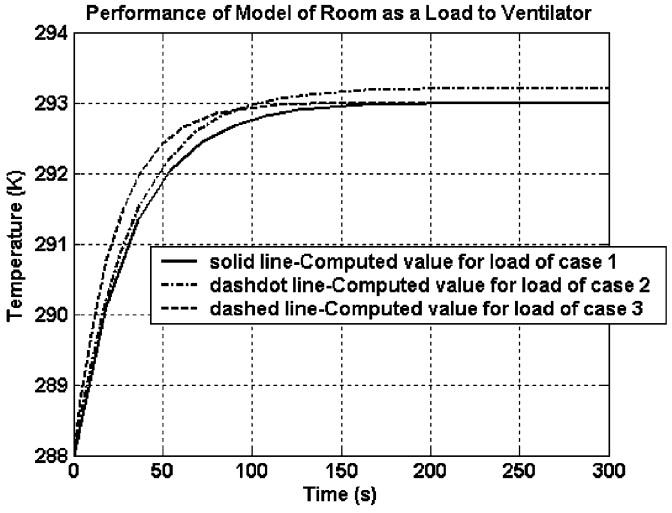

Fig. 21. Performance comparison for room air model under three kinds of conditions.

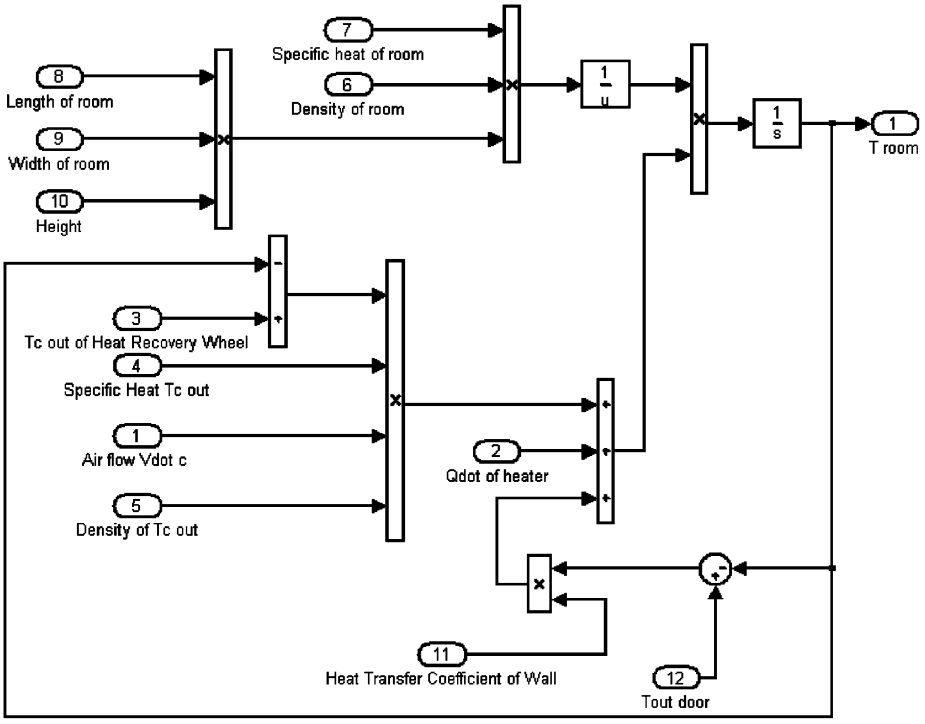

Fig. 20. Schematic diagram of model for air inside room in SIMULINK.

supply air (J/kg K), V_{induct} is the volume of the air inside duct (m^3), T_s—is the temperature of supply air (K) (Fig. 23).

$$\dot{m}_c c_{p,c}(T_{c,out} - T_s) + \dot{Q}_{heater} = c_{p,s} \cdot L_{duct} \cdot A_{duct} \cdot \rho_s \cdot \frac{dT_s}{dt}, \quad (25)$$

where $\dot{m}_c$ is the mass flow rate of cold air (kg/s), $c_{p,c}$ is the specific heat of cold air from the heat recovery section (J/kg K), $T_{c,out}$ is the temperature of the cold air from the heat recovery section (K), A_{duct} is the area inside the duct (m^2), ρ_s is the density of supply air from the duct (kg/m^3), and other parameters are specified in Nomenclature.

For the model of the duct air, the main affecting factors are airflow, material and shape of the duct, friction resistance, and whether the heater is on or off. The comparison of the performance of the model of air inside duct under different conditions are presented in Fig. 24. These results were obtained by varying the above dominant factors.

More precisely, there are three detection cases of operating conditions to compare the simulation performance with variable inputs. The initial condition of the temperature of the air inside duct was set at 278 K.

Case No. 1: The heater is off, and the length of duct is one meter.

Case No. 2: The heater is on, the energy is 100 J, duct is 5 m long (this will increase the pressure drop correspondingly).

Case No. 3: The heater is off, airflow from ventilator increases from 0.25 to 0.35.

By analyzing the results the following conclusions can be drawn. Temperature will reach the highest level when the

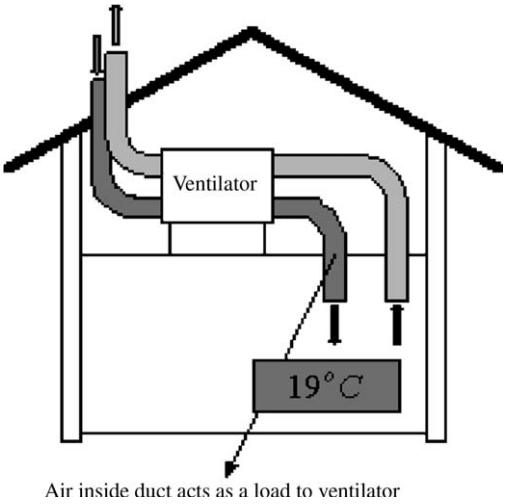

Fig. 22. Air inside duct being a load to ventilation unit for supply air temperature regulation.

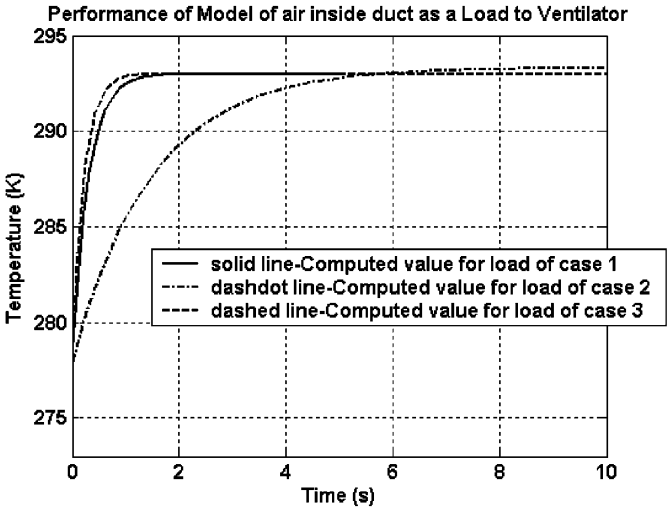

Fig. 24. Performance comparison for duct air model under three kinds of conditions.

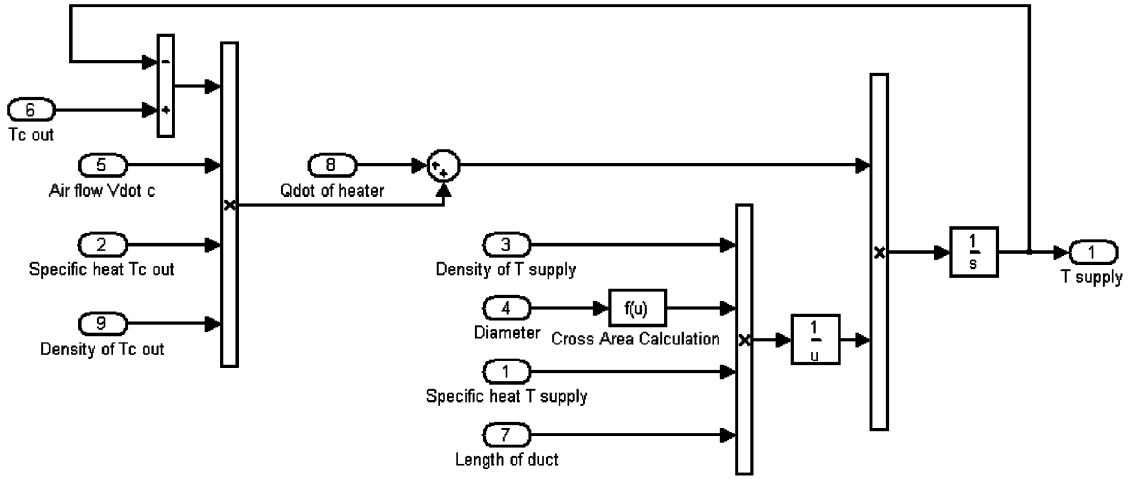

Fig. 23. Schematic diagram of model for air inside duct.

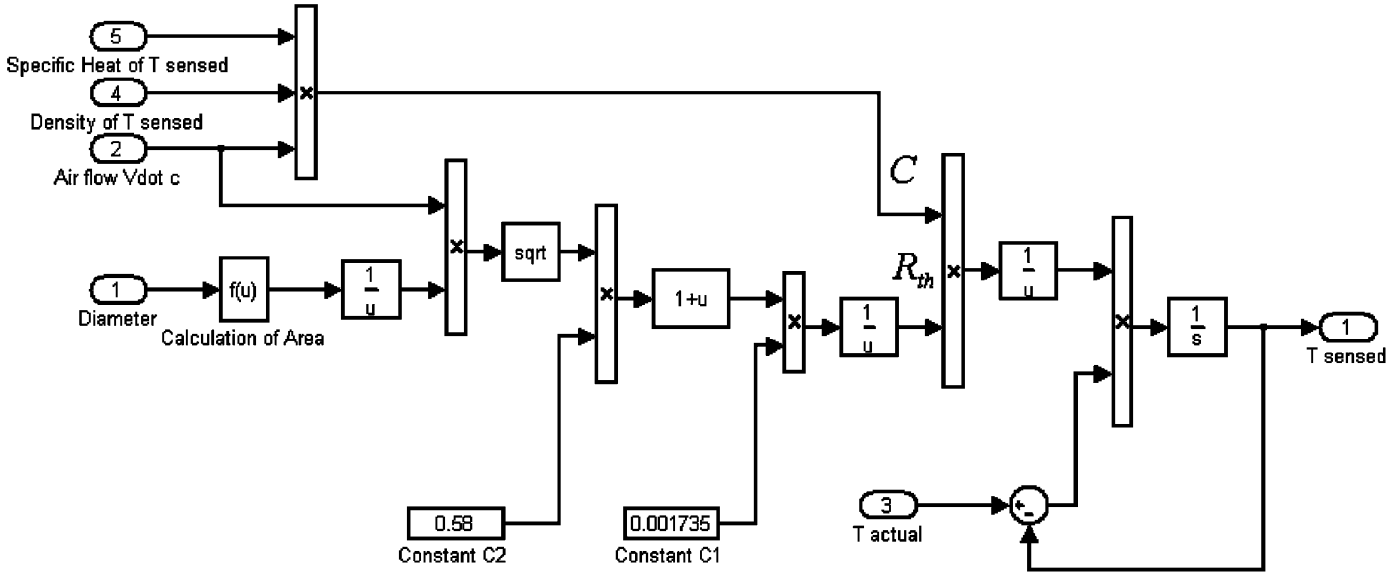

Fig. 25. Schematic diagram of model for temperature sensor.

heater is on, even though the length of the duct is long which will increase the pressure drop. The reacting time is large compared with other conditions because of the large volume of the air inside the duct. Temperature response effectiveness increases when airflow increases with specified heat conduction coefficient.

Our final remarks will be related to the model of the temperature sensor which can be developed as follows:

$$T_{\text{out}} = \frac{1}{R_{\text{th}} C} \int (T_{\text{in}} - T_{\text{out}})\, \mathrm{d}t, \tag{26}$$

$$R_{\text{th}}(v) = \frac{1}{s_1 (1 + s_2 \cdot \sqrt{v})} = \frac{1}{s_1 \left(1 + s_2 \cdot \sqrt{\dfrac{\dot{v}}{A}}\right)}, \tag{27}$$

where T_{in} is the actual (real) temperature which needs to be sensed (that is the input of the sensor), T_{out} is the sensed temperature (that is the output of the sensor), the thermal capacity $C = \dot{m} c_{\text{p}} = \dot{v} \rho c_{\text{p}}$ and the thermal resistance $R_{\text{th}}(v)$ are determined by the velocity of airflow $\dot{v}$ which flows through the sensor. From experiments, the constants s_1, s_2 are determined to be 0.001735 and 0.58, respectively. The model identify the thermal resistance coefficient $R_{\text{th}}(v)$ as a function of airflow. The corresponding function block was constructed in SIMULINK and shown in Fig. 25.

Models for the airflow control system, loading conditions, sensors developed here supplemented by a model for the heat exchanger provide a way to construct the entire regulation system for the ventilation unit.

6. Conclusions

In this paper we focused on the model-based analysis and simulation of the airflow control system of a typical ventilation unit operating in building environments. We considered essential block components of the system together with conventional PI controller implementations. The dynamic responses obtained from simulations with mathematical models developed for each such a block have been compared with the measurement and experimental data. We analyzed the performance of the constant airflow control scheme and provided the results of the simulations for two typical loading conditions for the ventilation units installed in building environments. Aiming at the analysis and simulation of the behavior of the airflow control system for a typical ventilation unit operating in building environments, the main achievement of this work is the modeling and connection of individual components, and application of the PI controller for the entire air flow controlling system. The closed-loop dynamic performances have been compared with measurements demonstrating good agreement. Some important parameters have been identified through experiments. The obtained results showed that the designed control system is flexible enough to satisfy all the imposed constraints with varied operating and loading conditions in order to fulfill the thermal comfort requirements for the extract air from the room and supply air to the room.

References

[1] Alcala R, Benitez JM, Casillas J, Cordon O, Perez R. Fuzzy control of HVAC systems optimized by genetic algorithms. Applied Intelligence 2003;18:155–77.

[2] Ogata K. Modern control engineering. Upper Saddle River, NJ: Prentice-Hall; 1997.

[3] Liddament, Martin W. A guide to energy efficient ventilation. Coventry: University of Warwick Science Park, Air Infiltration and Ventilation Centre; 1996.

[4] Ned M, Undeland MT, Robbins PW. Power electronics: converters, applications, and design. New York: Wiley; 1995.
[5] Goodfellow H, Tahti A. Industrial ventilation design guidebook. New York: Academic Press; 2000.
[6] Sheets RGW. Encyclopedia of electronic circuits. New York: McGraw-Hill; 1992.
[7] UH3D Reference Manual. Program Version 3.1. Berkeley, CA: ICEM CFD Engineering; 2001.
[8] Bejan A. Heat transfer. New York: Wiley; 1993.
[9] Wu Z, Melnik RVN, Borup F. Model-based analysis and simulation of regenerative heat wheel. MCI technical report, University of Southern Denmark; 2003. p. 1–26.